WIND RESISTANCE PERFORMANCE ANALYSIS OF A FLAT-ELLIPTICAL PIPE GREENHOUSE FRAME
/
平椭圆管塑料大棚骨架抗风性能分析

Cunxing WEI[1)], Hengyan XIE[2,*)], Xin ZHENG[2)], Wenbao XU[2)]
[1)] College of Engineering, Heilongjiang Bayi Agricultural University, Daqing 163319, China
[2)] College of Civil Engineering and Water Conservancy, Heilongjiang Bayi Agricultural University, Daqing 163319, China
Tel: +86-459-13766785587; E-mail: xiehy555@byau.cn
Corresponding author: Hengyan Xie
DOI: https://doi.org/10.35633/inmateh-77-101

Keywords: *flat-elliptical pipe greenhouse frame; finite element modeling; linear filtering method; fluctuating wind load; wind-induced vibration response*

ABSTRACT
This study investigates the wind resistance performance of a novel flat-elliptical pipe greenhouse by developing a finite element model of the greenhouse frame using ABAQUS software. Based on the Davenport fluctuating wind speed spectrum and the Shiotani correlation coefficient, a MATLAB program was developed using an autoregressive (AR) model within a linear filtering method to simulate fluctuating wind speed time-history curves. Both static and full dynamic wind loads were applied to the model to evaluate the wind resistance performance of greenhouse frames with 5 arches and 50 arches. The results indicate that under static wind loading, the stresses in the frames did not exceed the elastic limit, and the deformations remained within the allowable range. However, under full dynamic wind loading, the stresses in the frames exceeded the elastic limit and entered the plastic stage. Although the lateral displacement in the plastic stage remained within permissible limits, the overall structure failed to meet the safety requirements of the greenhouse.

摘要
本研究针对新型平椭圆管塑料大棚，利用 ABAQUS 有限元软件建立了大棚骨架模型。基于 Davenport 脉动风速谱，选择 Shiotani 相关系数，采用线性滤波法中的 AR 法（自回归模型）编写 MATLAB 程序对脉动风速时程曲线进行了模拟。分别对模型施加静力风荷载和全动力风荷载，分析得到五榀和五十榀平椭圆管骨架塑料大棚抗风性能，分析结果表明：在静力风荷载作用下，大棚及骨架应力均未超过弹性极限，变形均在容许值范围内；在全动力风荷载作用下，大棚及骨架应力超过弹性极限，进入塑性阶段，但塑性阶段侧移未超过容许值，不满足大棚结构安全性要求。

INTRODUCTION
Greenhouses, although designed and constructed based on principles of civil engineering, lack comprehensive national standards compared with conventional civil structures. Consequently, the specifications of greenhouse frames vary widely, and many are manufactured by small workshops with inadequate quality control. These substandard frames often exhibit insufficient load-bearing capacity, resulting in frequent structural failures under extreme weather conditions, such as strong winds or heavy snowfall, which cause substantial threats to human safety and significant losses in agricultural production *(Briassoulis, 2016; Ryu, 2019; Uematsu, 2020)*. In contrast to earlier periods, when economic efficiency was the primary concern, growers are now increasingly inclined to adopt greenhouse structures that offer higher levels of safety, durability, and overall cost-effectiveness *(Huang, 2024; Xie, 2025)*. In response to this demand, a new type of greenhouse characterized by a flat-elliptical pipe frame has been developed and is now widely adopted in cold northern regions of China.

Compared with truss-type greenhouse frames, flat-elliptical pipe greenhouse frames offer several advantages, including ease of fabrication, rapid installation, reliable connections, and improved structural stability.

Cunxing Wei, Ph.D. Eng.; Hengyan Xie, Prof. Ph.D. Eng.; Xin Zheng, Prof. Ph.D. Eng.; Wenbao Xu, Ph.D. Eng.

In addition, compared with circular steel pipes, flat-elliptical pipes exhibit larger moments of inertia and higher stiffness, thereby enhancing the structural resistance to external loads.

Relative to truss arches, flat-elliptical pipe greenhouse frames provide a more economical solution due to their simpler manufacturing process, convenient construction, and favorable cost-performance ratio. Despite these advantages, research on this type of greenhouse remains limited, and standardized design guidelines and theoretical foundations are still lacking, which restricts its wider application and promotion. Nevertheless, according to manufacturers and practitioners, this structural form exhibits superior resistance to wind and snow loads, making it the predominant greenhouse type in cold northern regions *(Yan, 2022)*. The geometry of the flat-elliptical pipe and its cross-section is illustrated in Fig. 1.

a) Flat-elliptical pipe ***b) Diagram of cross-section***

Fig. 1 – Flat-elliptical pipe and its cross-section

Previous studies analyzing greenhouse wind resistance have primarily relied on simplifying wind action into equivalent static loads for structural response assessment *(Ha, 2017; Ren, 2019; Kim, 2024)*. While such approaches offer computational convenience, they inherently neglect the stochastic and fluctuating nature of wind, resulting in limitations when applied to the safety evaluation of flexible structures such as greenhouses *(Takeshi, 2017; Vieira, 2020; Xu, 2023; Xie, 2025)*. To address these shortcomings, many researchers have turned to spectral methods in recent years, particularly the use of the Davenport spectrum, to simulate fluctuating wind fields and investigate wind-induced dynamic responses of lightweight structures *(Davenport, 1961; Li, 2022; Wang, 2023)*. Nevertheless, research focusing specifically on the wind resistance performance of flat-elliptical pipe greenhouse frames remains limited. In addition, standardized design guidelines and theoretical foundations for their structural design are lacking, which hinders their wider application and promotion.

This study is the first to integrate an autoregressive (AR) - based linear filtering simulation of spatially correlated fluctuating wind fields with full dynamic finite element analysis in ABAQUS for flat-elliptical pipe greenhouse frames. The proposed approach enables (1) realistic time-domain stochastic wind loading with spatial correlation based on Shiotani coefficients and allows (2) the direct application of full dynamic wind-pressure time histories to solid-element (C3D8R) finite element models incorporating elasto-plastic material behavior. Furthermore, (3) the dynamic responses of short-span (5-arch) and long-span (50-arch) greenhouse frames under identical stochastic wind scenarios are comparatively evaluated, providing a novel contribution to structural design guidance and wind-induced risk assessment for this greenhouse type.

This study aims to establish a finite element model of a flat-elliptical pipe greenhouse frame using ABAQUS software. A spatially correlated fluctuating wind field is generated in MATLAB, and the simulated fluctuating wind speed is superimposed on the mean wind speed to obtain a full dynamic wind speed time history, which is subsequently converted into a corresponding time history of full dynamic wind loads. Both static wind loads and full dynamic wind loads are then applied to finite element models of greenhouse frames consisting of 5 arches and 50 arches, respectively, in ABAQUS. The stress distribution and structural performance of the greenhouse frame under different wind loading conditions are analyzed, providing a systematic evaluation of the wind resistance behavior of flat-elliptical pipe greenhouse frames. The results are expected to offer theoretical support for structural optimization and the safe promotion of this greenhouse type in regions frequently affected by extreme climatic events.

MATERIALS AND METHODS

Finite element model

In this study, a full-scale finite element model of the flat-elliptical pipe greenhouse frame was developed using ABAQUS 2016. A photograph of the flat-elliptical pipe greenhouse frame is shown in Fig. 2(a), and the corresponding dimensional schematic is presented in Fig. 2(b).

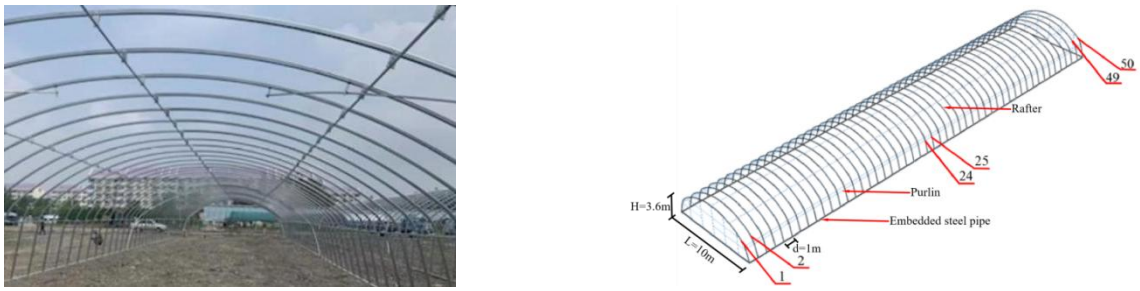

a) Skeleton photo *b) Schematic diagram of skeleton dimensions*

Fig. 2 – Flat-elliptical pipe greenhouse

Meshing and boundary conditions

To investigate the elasto-plastic behavior and perform nonlinear analysis, the flat-elliptical pipe greenhouse frame was modeled using solid elements. Specifically, C3D8R eight-node linear brick elements were selected based on the structural characteristics of the members.

The flat-elliptical pipe arches were welded to embedded steel pipes at the rafter bases, resulting in relatively high support stiffness for the greenhouse frame. Accordingly, in the finite element model, the rafter bases were rigidly connected to the embedded steel pipes, and the rafters were tied to the purlins. All translational and rotational degrees of freedom at the rafter bases were constrained to simulate fixed boundary conditions.

Material parameter

In this study, the greenhouse frame is constructed from Q235B galvanized steel pipes, which provide adequate strength, stiffness, and corrosion resistance, thereby ensuring reliable support for the greenhouse film under wind loading conditions. The greenhouse covering material is polyolefin (PO) film, which is widely used in practical engineering applications. The film-tensioning lines are primarily composed of polyamide (PA), commonly known as nylon, a high-performance synthetic fiber characterized by good wear resistance and elasticity. The material parameters of the main structural components of the flat-elliptical pipe greenhouse are summarized in Table 1.

Table1

Material parameters of the greenhouse frame, film, and film-tensioning lines

Component	b×h or R (mm)	t (mm)	ρ (kg/m^3)	f_y (MPa)	λ	E (MPa)
Rafter	30×60	2	7.85	235	0.28	2.1×10^5
Embedded steel pipe	30×80	2	7.85	235	0.28	2.1×10^5
Purlin	ϕ 20	2	7.85	235	0.28	2.1×10^5

Calculation of mean wind speed

The plastic greenhouse considered in this study is located in Jiamusi, Heilongjiang Province, China. According to the Chinese standard *Load Code for the Design of Building Structures* (MOHURD, 2016), the design service life of a plastic greenhouse is 10 years, and the basic wind pressure in Jiamusi corresponding to a 3-s gust is 0.38 kN/m^2.

However, according to the Chinese standard *Load Code for Design of Building Structures* (*MOHURD, 2012*), the basic wind pressure in Jiamusi for a 50-year return period at a 10-min averaging interval is 0.65 kN/m^2.

According to the Chinese standard *(MOHURD, 2016)*, the ratio of wind pressure corresponding to a 10-year return period to that of a 50-year return period is 0.734. Therefore, the basic wind pressure for a 10-year return period at a 10-min averaging interval is 0.65×0.734=0.477 kN/m^2.

According to Bernoulli's principle in fluid mechanics, the relationship between wind pressure and wind speed can be expressed as:

$$w = \frac{1}{2}\rho v^2 = \frac{\gamma}{2g}v^2 \tag{1}$$

where w is the wind pressure, kN/m^2, ρ is the air density, kg/m^3, v *is* the wind speed, m/s, γ is the air gravity density, kN/m^3, g is the gravitational acceleration, m/s^2.

In Eq. (1), the air density ρ is taken as 0.012018 kg/m^3 under the standard atmospheric pressure of 101.235kPa. Jiamusi is located near 45° north latitude; therefore, the gravitational acceleration is taken as g=9.8 m/s^2. Under these conditions, the wind pressure can be can be expressed as:

$$w = \frac{1}{2}\rho v^2 = \frac{0.012018}{2\times 9.8}v^2 = \frac{v^2}{1630} \tag{2}$$

According to the relationship between wind pressure and wind speed, the mean wind speed at a standard height of 10 m, for terrain category B, a 10-year return period, and a 10-min averaging interval, is calculated to be 27.88 m/s.

The standard value of the static wind load acting perpendicular to the building surface is calculated using the following expression (3):

$$w = \beta_z \mu_s \mu_z w_0 \tag{3}$$

where w is the standard value of wind load, kN/m^2, β_z is the wind vibration coefficient at height z, μ_s is the wind load shape coefficient, which is shown in Fig. 3(a), μ_z is the height variation coefficient of wind pressure, w_0 is the basic wind pressure, kN/m^2.

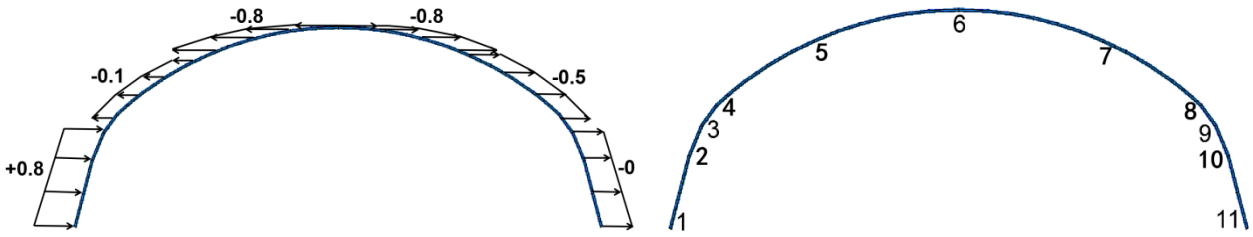

a) Wind load shape coefficient *b) Diagram of load application points*

Fig. 3 - Wind load shape coefficient and load application points of the greenhouse frame

Meanwhile, to facilitate the description of the structural positions in the subsequent sections, the transverse arches of the greenhouse frame were sequentially numbered from the windward base to the leeward base, resulting in 11 reference points, as illustrated in Fig. 3(b).

Simulation of fluctuating wind speed

The simulations were conducted using MATLAB R2021a for the generation of fluctuating wind speed time histories and ABAQUS/Standard 2016 for finite element static and dynamic analyses. Fluctuating wind speed can be modeled as a Gaussian stationary random process and simulated using the linear filtering method.

The autoregressive (AR) method is a specific type of linear filtering technique that offers the advantages of simple computation, high accuracy, and fast convergence, making it well suited for simulating fluctuating wind

speed time histories. The fundamental principle of the AR method is to predict future values of a time series based on its previous data.

The time history of fluctuating wind speed for M points AR model in space can be expressed as follows:

$$V(X,Y,Z,t) = \sum_{k=1}^{p} \psi_k V(X,Y,Z,t-K\Delta t) + N(t) \quad (4)$$

where $X = (x_t,\ldots,x_m)^T, Y = (y_t,\ldots,y_m)^T, Z = (z_t,\ldots,z_m)^T$ are the 3-D coordinates of M-points in space, $V(X,Y,Z,t)$ is the $M \times 1$ fluctuating wind speed vector at time t, K is the surface drag coefficient, p is the order of AR model, Δt is the time step used for wind speed simulation, ψ_k is the autoregressive coefficient matrix of AR model, $k = 1,\ldots,p$; $N(t)$ is the variable in independent random process.

The Davenport fluctuating wind speed spectrum yields relatively conservative results in the high-frequency range, thereby providing a higher level of structural safety. Consequently, the Davenport wind power spectrum is adopted in this study to simulate the fluctuating wind acting perpendicular to the greenhouse surface, which can be expressed as:

$$S_v(f) = \overline{V}_{10}^2 \frac{4Kx}{f(1+x^2)^{4/3}} \quad (5)$$

$$x = 1200\frac{f}{\overline{V}_{10}} \quad (6)$$

where:

$S_v(f)$ is the auto-power of the fluctuating wind speed, f is the wind-speed fluctuation frequency, K is the surface drag coefficient, $\overline{V}_{10}$ is the mean wind speed at a height of 10 m with a 10-min averaging interval, x is the turbulence integral scale parameter, taken as 0.02 in the Davenport fluctuating wind speed spectrum.

Referring to the experience and methods reported by researchers both domestically and internationally for simulating fluctuating wind speed time-history curves of large-span structures, and in combination with the time-domain analysis method, only the spatial position was selected as the independent variable in this study due to the relatively small span of the flat-elliptical pipe plastic greenhouse. The spatial correlation of fluctuating wind speed in the longitudinal (x-direction) and vertical (z-direction) directions of the greenhouse was considered. The Shiotani correlation coefficient was adopted to simulate the fluctuating wind speed time-history curves, which can be expressed as:

$$\mathrm{coh}\left(x,x'\right) = \exp\left(-\frac{|x-x'|}{L_x}\right), \mathrm{coh}\left(z,z'\right) = \exp\left(-\frac{|z-z'|}{L_z}\right) \quad (7)$$

where L_x is the integral scale of turbulence in the x-direction, taken as 50 m, L_z is the integral scale of turbulence in the z-direction, taken as 60 m.

Based on the experience and conclusions of previous studies and multiple trial simulations with different parameters, the simulation parameters for the fluctuating wind speed were determined as follows: the mean wind speed at a height of 10 m in Jiamusi, Heilongjiang Province, corresponding to a 10-year return period, was 27.88 m/s; the autoregressive (AR) model order was set to 4; the total simulation duration was 60 s with a time step of 0.1 s; the upper cut-off frequency was 10 Hz with a frequency increment of 0.01 Hz; and the surface drag coefficient K was taken as 0.003.

Based on the simulated fluctuating wind speed time histories at the spatial points, the full dynamic wind speed time-history curves were obtained by superimposing the fluctuating wind speed on the mean wind speed. Using the conversion relationship between wind speed and wind pressure, the corresponding full dynamic wind load time-history curves were then derived. The wind load time histories at the top point of the central greenhouse arch and the end greenhouse arch are illustrated in Fig. 4.

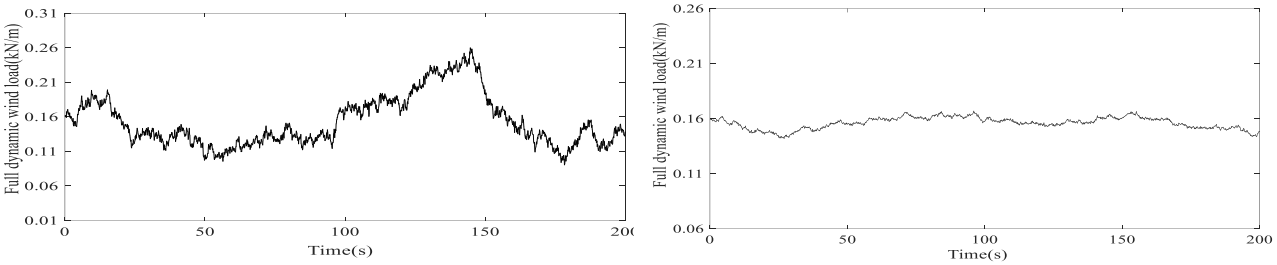

a) Top point on the central greenhouse arch *b) Top point on the end greenhouse arch*

Fig. 4 - Full dynamic wind load time-history curves

RESULTS

According to the *Chinese standard (MOHURD, 2017)*, the stresses and displacements of the flat-elliptical pipe greenhouse frame evaluated under elastic analysis should satisfy the following safety requirements in the elastic stage:

(1) Stress: The stress in the greenhouse frame members must be lower than the material yield strength. Specifically, the stress in the arch members shall not exceed 235 MPa.

(2) The vertical displacement of the greenhouse frame must be less than the allowable limit $[l_T] = 10000/400 = 25\text{mm}$. In addition, the horizontal displacement at the top of the greenhouse arch must also remain within the permissible value $[h] = 36000/1500 = 24\text{ mm}$.

These criteria ensure that the flat-elliptical pipe greenhouse frame remains within the elastic range and satisfies the structural safety requirements under the applied wind loads.

Stress analysis under static wind load

The static wind load obtained in the previous section was applied to the finite element model of the flat-elliptical pipe greenhouse frame to evaluate its structural response. Since identical wind loads were uniformly applied to all greenhouse arches under static analysis, and the influence of the gable-end arches was not considered, the load response of each arch was identical and independent of the total number of arches.

The stress distribution and displacement contours of the central arch in the 5-arch greenhouse frame are presented in Fig. 5.

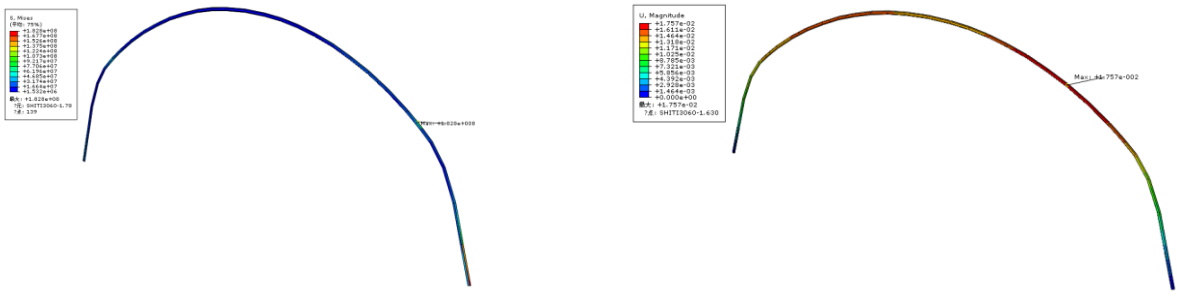

a) Stress distribution *b) Displacement distribution*

Fig. 5 - Stress and displacement distributions of the central greenhouse arch in the 5-arch configuration

As shown in Fig. 5(a), the maximum stress of the greenhouse frame reached 182.8 MPa, occurring at the shoulder region of the arch on the leeward side. Figure 5(b) shows that the vertical displacement of the frame was 17.57 mm, which is less than the allowable vertical displacement and also occurred in the shoulder region on the leeward side. Using the built-in query tool in ABAQUS, the horizontal displacement at the top of the greenhouse arch was determined to be 12.35 mm, which is below the allowable horizontal displacement, indicating that the horizontal displacement remained within permissible limits. The stress distribution and displacement diagrams of the center arch in the 50-arch greenhouse frame are presented in Fig. 6.

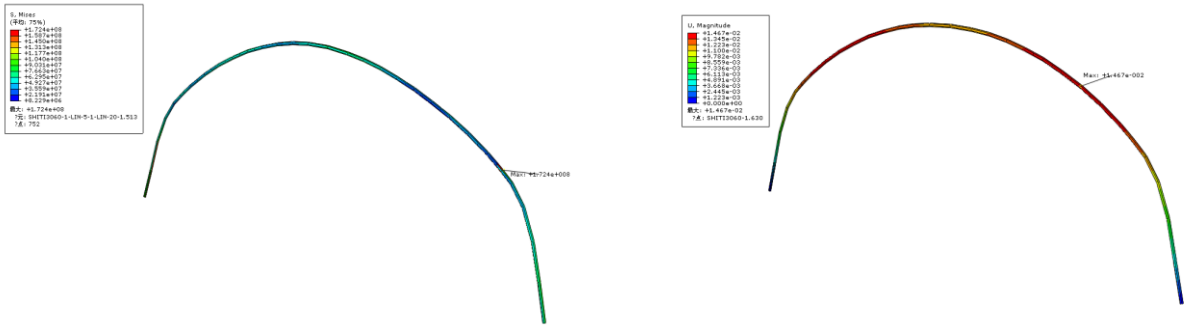

a) Stress distribution *b) Displacement distribution*

Fig. 6 - Stress and displacement distributions of the central arch in the 50-arch greenhouse frame

As shown in Fig. 6(a), the maximum stress of the greenhouse frame was 172.4 MPa, occurring at the shoulder region on the leeward side of the arch. Figure 6(b) shows that the vertical displacement of the frame was 14.67 mm, which is below the allowable vertical displacement and also occurred at the shoulder region on the leeward side. The horizontal displacement at the top of the arch was 10.24 mm, which is less than the allowable horizontal displacement, indicating that the horizontal movement remained within permissible limits.

Stress analysis of flat-elliptical pipe greenhouse frames under full dynamic wind load

To investigate the stress variation and correlation characteristics of greenhouse frames consisting of 5 arches and 50 arches under full dynamic wind loading, full dynamic wind loads were applied to the corresponding finite element models. Subsequently, a point-by-point stress comparison was conducted to analyze the distribution and correlation of stress responses among the arches. When applying full dynamic wind loads to the greenhouse frames, the spatial autocorrelation of horizontal fluctuating wind must be considered. As a result, the full dynamic wind load acting on the central arch is slightly higher than that on the adjacent arches and significantly higher than that on the end arches.

The loading and boundary conditions for the full dynamic wind analysis of the greenhouse frame with 5 arches are illustrated in Fig. 7(a). The full dynamic wind load was applied to the 5-arch greenhouse frame, and the resulting stress distribution is shown in Fig. 7(b). The stress values at each monitoring point on the central arch were extracted and are summarized in Table 2.

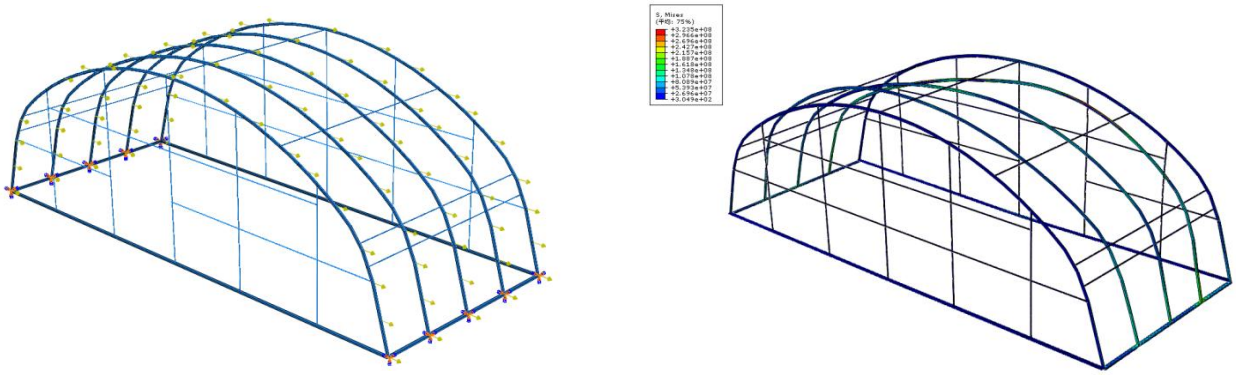

a) Load positions and boundary conditions *b) Stress distribution*

Fig. 7 - Load positions, boundary conditions, and stress distribution of the 5-arch greenhouse frame under full dynamic wind load

Table 2

Stress values at selected points on the central arch under full dynamic wind load

Point	Point location	Stress (MPa)
1	Windward bottom	28.66
3	Windward waist	156.7
5	Windward shoulder	199.2
6	Arch crown	244.5
7	Leeward shoulder	315.2
9	Leeward waist	216.9
11	Leeward bottom	44.68

As shown in Table 2, the maximum stress among all points on the central greenhouse arch occurred at Point 7, followed by Point 6, while the two bottom points exhibited the lowest stress values. The maximum stress of the greenhouse frame reached 323.5 MPa, occurring between the top and shoulder regions on the leeward side, approximately corresponding to Point 7. Overall, the stress along the greenhouse arch increased gradually from the windward bottom toward the leeward shoulder region. This stress distribution can be attributed to the spatial autocorrelation and randomness of the fluctuating wind field and is consistent with stress patterns reported in previous studies *(Wang, 2022)*.

The loading and boundary conditions for the full dynamic wind load applied to the 50 greenhouse arches are illustrated in Fig. 8(a), and the corresponding stress distribution is shown in Fig. 8(b). The stress values at each monitoring point on the central greenhouse arch were extracted and are presented in Table 3.

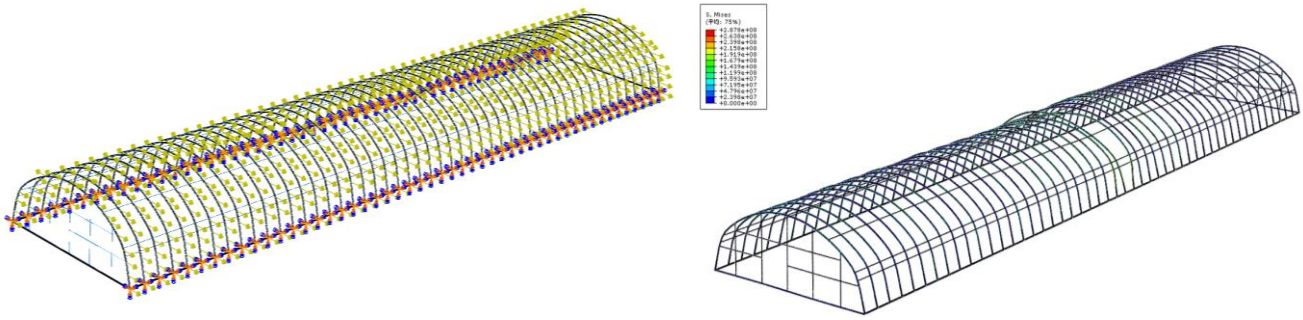

a) Load positions and boundary conditions ***b) Stress distribution***

Fig. 8 – Load positions, boundary conditions, and stress distribution of the 50-arch greenhouse frame

Table 3

Stress values at each point of the central greenhouse arch under full dynamic wind load

Point	Point location	Stress(MPa)
1	Windward bottom	18.6
3	Windward waist	164.3
5	Windward shoulder	185.2
6	Arch crown	233.8
7	Leeward shoulder	268.3
9	Leeward waist	186.2
11	Leeward bottom	33.41

As shown in Table 3, the maximum stress among all points on the central greenhouse arch occurred at Point 7, followed by Point 6, while the lowest stress values were observed at the two bottom points. The maximum stress of the greenhouse frame reached 287.8 MPa, occurring in the region between the arch crown and the leeward shoulder, approximately corresponding to Point 7. Overall, the stress along the greenhouse arch exhibited a gradually increasing trend from the windward bottom toward the leeward shoulder, which is consistent with the stress distribution pattern observed in the 5-arch greenhouse configuration.

DISCUSSION

Spatial correlation and dynamic amplification: The observed stress concentration at the leeward shoulder (Point 7) is primarily attributed to the combined effects of the mean wind pressure gradient along the greenhouse arch and the stochastic fluctuating wind component with spatial autocorrelation. Due to the positive spatial correlation near the center arch, fluctuating wind-speed peaks at adjacent points tend to occur simultaneously, which amplifies the local bending moment at the leeward shoulder.

To evaluate numerical convergence, mesh sensitivity analyses were conducted on a representative center arch segment. Three mesh densities were examined: a coarse mesh with an element size of 20 mm, a medium mesh with an element size of 10 mm, and a fine mesh with an element size of 5 mm. The relative difference in peak von Mises stress between the medium and fine meshes was less than 3%, indicating satisfactory numerical convergence. Consequently, the medium mesh was selected for subsequent parametric analyses as an appropriate balance between computational efficiency and accuracy.

Uncertainties in the present analysis mainly stem from the selection of turbulence parameters, aerodynamic coefficients, material property variability, and damping assumptions. Nevertheless, comparison with previous studies *(Li, 2022; Wang, 2023)* shows that the overall stress distribution patterns are consistent, particularly with respect to stress concentration locations. Differences in absolute stress magnitudes are primarily due to variations in structural geometry and boundary conditions.

CONCLUSIONS

This study investigated the structural behavior of 5-arch and 50-arch flat-elliptical pipe greenhouse frames under static and full dynamic wind loads using finite element analysis. The main conclusions are as follows:

(1) Static wind load response: Both the 5-arch and 50-arch greenhouse frames exhibited stresses and displacements within the allowable limits under static wind loading, remaining in the elastic range and satisfying structural safety requirements.

(2) Full dynamic wind load response: Under full dynamic wind loading, both the 5-arch and 50-arch greenhouse frames exceeded the allowable stress limits and entered the plastic stage, indicating that the structural safety requirements were not satisfied.

(3) Stress distribution and critical locations: The maximum stress consistently occurred at the leeward shoulder of the central greenhouse arch, with stress gradually increasing from the windward base toward the leeward shoulder. This distribution reflects the combined effects of wind turbulence and spatial correlation of the fluctuating wind field.

(4) Effect of greenhouse length: Compared with the 5-arch model, the 50-arch model exhibited lower stress and displacement responses, highlighting the importance of considering the full greenhouse length and spatial wind correlation effects in structural analysis.

In conclusion, full dynamic wind analysis is essential for the safe design of flat-elliptical pipe greenhouse frames, particularly for long-span configurations. The findings of this study provide a theoretical basis for structural optimization, standardization, and reliable application of this greenhouse type in regions prone to extreme wind and snow loads. The present analysis is based on idealized boundary conditions and does not consider the elastic characteristics of greenhouse frame supports. Future studies should incorporate structural damping and realistic support flexibility to quantify their mitigating effects on dynamic amplification. In addition, experimental validation of the stochastic wind input and dynamic structural responses is recommended.

ACKNOWLEDGEMENTS

This study is supported by Natural Science Foundation of Heilongjiang Province of China (LH2019E072). All authors are grateful for this support.

REFERENCES

[1] Briassoulis. D., Dougka, G., Dimakogianni, D., & Vayas, I., (2016). Analysis of the collapse of a greenhouse with vaulted roof. *Biosystems Engineering*. Vol. 151, pp. 495-509, England. DOI: https://doi.org/10.1016/j.biosystemseng.2016.10.018

[2] Davenport, A. G. (1961). The spectrum of horizontal gustiness near the ground in high winds. *Quarterly Journal of the Royal Meteorological Society*. Vol. 87, No. 372, pp. 194-211, England. DOI: https://doi.org/10.1002/qj.49708737208

[3] Ha, T., Kim, J., Cho, B-H., Kim, D-J., (2017). Finite element model updating of multi-span greenhouses based on ambient vibration measurements. *Biosystems Engineering*. Vol. 161, pp. 145-156, England. DOI: https://doi.org/10.1016/j.biosystemseng.2017.06.019

[4] Huang, B., Liu, J., Li, Z., (2024). Analysis of wind pressure characteristics of typical agricultural greenhouse buildings on tropical islands. *Advances in Aerodynamics.* Vol. 6, No. 1, pp. 1-21, Germany. DOI: https://doi.org/10.1186/s42774-023-00170-0

[5] Kim H-K, (2024). Evaluating the Ventilation Performance of Single-Span Plastic Greenhouses with Continuous Screened Side Openings. *Agronomy*. Vol. 14, No.7, Switzerland. DOI: https://doi.org/10.3390/agronomy14071447

[6] Li, X., Wang C., Jiang Y., Bai, Y. (2022). Dynamic response analysis of a whole steel frame solar greenhouse under wind loads. *Scientific reports*. Vol. 12, pp. 1-12, England. DOI: https://doi.org/10.1038/s41598-022-09248-z

[7] MOHURD. (2012). *GB 50009-2012 Load code for the design of building structures.* (建筑结构荷载规范). Beijing, China: China Architecture & Building Press (in Chinese). DOI: https://www.mohurd.gov.cn/gongkai/fdzdgknr/tzgg/201207/20120723_210754.html.

[8] MOHURD. (2016). *GB/T 51183-2016 Code for the design load of horticultural greenhouse structures*. （农业温室结构荷载规范）. Beijing/China: China Planning Press (in Chinese). https://www.mohurd.gov.cn/gongkai/zhengce/zhengcefilelib/201702/20170214_230578.html.

[9] MOHURD (2017). *GB 50017-2017 Code for design of steel structures* (钢结构设计标准). Beijing/China: China Architecture & Building Press (in Chinese).

[10] Ren, J., Wang, J., Guo, S., Li, X., Zheng, K., & Zhao, Z., (2019). Finite element analysis of the static properties and stability of a large-span plastic greenhouse. *Computers and Electronics in Agriculture.* Vol. 165, pp. 1-9, England. DOI: https://doi.org/10.1016/j.compag.2019.104957

[11] Ryu, H R., Choi, M K., Cho, M W., (2019). Damage index estimation by analysis of meteorological disasters on film plastic greenhouses. *International Journal of Agricultural and Biological Engineering*, Vol. 12, pp. 58-63. Beijing/China. DOI: https://doi.org/10.25165/j.ijabe.20191205.4493

[12] Takeshi Kuroyanagi, (2017). Investigating air leakage and wind pressure coefficients of single-span plastic greenhouses using computational fluid dynamics. *Biosystems Engineering*. Vol. 163, pp. 15-27, England. DOI: https://doi.org/10.1016/j.biosystemseng.2017.08.004

[13] Vieira Neto, J.G., Soriano, J., (2020). Computational modelling applied to predict the pressure coefficients in deformed single arch-shape greenhouse. *Biosystems Engineering*, Vol. 200, pp. 231-245, England. DOI: https://doi.org/10.1016/j.biosystemseng.2020.10.003

[14] Uematsu, Y., & Takahashi, K., (2020). Collapse and reinforcement of pipe-framed greenhouse under static wind loading. *Journal of Civil Engineering and Architecture*, Vol. 14, pp. 583-594, United States. DOI: https://doi.org/10.17265/1934-7359/2020.11.001

[15] Wang, C., Jiang, Y., Wang, T., Xu Z., Bai, Y., (2022). Analysis of wind-induced responses of landing assembled Chinese solar greenhouses. *Biosystems Engineering*, Vol. 220, Issue 6, pp. 214-232. England. DOI: https://doi.org/10.1016/j.biosystemseng.2022.06.003

[16] Wang, C., Xu Z., Jiang, Y., Bai, Y., & Wang, T., (2023). Numerical analysis of static and dynamic characteristics of large-span pipe-framed plastic greenhouses. *Biosystems Engineering*, Vol. 232, No. 6, pp. 67-80, England. DOI: https://doi.org/10.1016/j.biosystemseng.2023.06.013

[17] Xie H., Wei C., Zheng X., Xu W., (2025). Stability analysis of flat-elliptical greenhouse skeleton considering initial geometrical imperfections. *INMATEH - Agricultural Engineering*, Vol. 75, No. 1, pp. 369-379, Bucharest/Romania. DOI: https://doi.org/10.35633/inmateh-76-31

[18] Xie Q., Ren J., (2025). Research on greenhouse planting density of landscape flowers in cold regions based on CFD simulation, *INMATEH - Agricultural Engineering*, Vol. 75, No. 1, pp. 469-479, Bucharest/Romania. DOI: https://doi.org/10.35633/inmateh-75-40

[19] Xu Y., Li Y., Song H., (2023) Large-span M-shaped greenhouse with superior wind resistance and ventilation performances. *Journal of Wind Engineering and Industrial Aerodynamics*, Vol. 238, No. 105410. England. DOI: https://doi.org/10.1016/j.jweia.2023.105410

[20] Yan, D., Hu L., Zhou C., Yan J., (2022). Analysis of the performance of the oval tube arch of single-tube solar greenhouses (椭圆管单管拱架日光温室结构性能分析). *Transactions of the Chinese Society of Agricultural Engineering.* Vol. 38, No. 5, pp. 217-224, Beijing/China. DOI: https://doi.org/10.11975/j.issn.1002-6819.2022.05.026